Boiling Heat Transfer Performance of Three-dimensionally Ordered Microporous Copper with Modulated Pore Diameters

Quang N. Pham, Shiwei Zhang, Lin Cheng-Hui, Shuai Hao, and Yoonjin Won
Department of Mechanical and Aerospace Engineering
University of California, Irvine
Irvine, California, USA, 92617
Email: won@uci.edu

ABSTRACT

There are significant interests in leveraging microporous surface for enhanced two phase cooling performance contributed by the entrapped vapor in pores and higher nucleation sites. However, the potentials for such porous media have yet to be realized due to the irregularity of the pore distributions and arrangement that are often used in boiling measurements. The lack of periodicity in pore packing limits the fundamental understanding of fluidic transport and bubble nucleation mechanics, making predictive modeling less accurate. Here, we report the pool boiling heat transfer performance of copper inverse opals, a microporous medium that exhibit a matrix of crystalline arranged pores. Various pore diameters of the inverse opals are investigated to provide insights into the boiling dynamics associated with porous structure morphologies. Increasing pore diameters show an increase in boiling heat transfer performance due to the combination of vapor permeability and sample thickness.

KEY WORDS: copper inverse opals, well-ordered pores, self-assembly, pool boiling, heat transfer coefficient

NOMENCLATURE

CHF	critical heat flux
d	diameter
h	heat transfer coefficient
k	conductivity
t	thickness
q"	heat flux
T	temperature
ΔT_{SH}	wall superheat temperature
R	thermal resistance
K	permeability
A	area

Subscripts

Au	gold
Cu	copper
IO	inverse opal
Si	silicon
sat	saturation
SH	superheat
TIM	thermal interface material
p	pore
v	via
dry	vapor layer
eff	effective
heat	heating

INTRODUCTION

The continually increasing power densities of high-performance electronics are bottlenecked by the challenges of thermal management [1]. Passive cooling with two-phase heat transfer has been shown to be an attractive solution for electronics cooling due to its utilization of the latent heat and lack of external pumping requirement. Liquid-vapor cooling operates by the cyclic transport of working fluid to a hot spot through a capillary wicking medium, which then induces boiling and evaporation phase change [2]. The enhancement of the heat transfer coefficient and critical heat flux (CHF) in pool boiling conditions has often been demonstrated through modification of surface morphologies and chemistries [3-6]. Extensive studies have reported on the boiling heat transfer enhancement of porous surfaces due to the combinations of increased solid-liquid surface area, capillary-assisted liquid feeding, increased nucleation site density, and availability of vapor escape routes. The open pores in three-dimensional porous surfaces effectively entrap vapor, reduce wall superheat [8], and provide bubble nucleation sites at low heat fluxes. While numerous studies have leveraged such advantages using metallic porous media in two phase heat transfer, the reported microporous structures often exhibit irregular pore distributions with polydisperse feature sizes [9,10]. The lack of highly-ordered pore packing limits the accuracy in predictive modeling of liquid flow and heat transfer [11-13]. Furthermore, random pore structures make correlating boiling mechanics to the associated pore morphologies difficult. Recent advances in colloidal template fabrication process provide opportunities to rationally design crystalline three-dimensional microporous structures with versatile level of tunability in pore sizes.

Inverse opal (IO) [14-18] is a porous media that exhibits an extremely ordered matrix of spherical pores derived from the sacrificial template of colloidal crystal. During the self-assembly of the templated spheres, the contact points between adjacent spheres become the interconnected windows between pores, denoted as the via, to create a continuous permeable network of pores. Fluid transport through the regular unit cells of IO has been modelled using finite element analysis [18,19] and quantified with experimental measurement [20]. The high permeability and large surface area-per-volume characteristics of IO structures make them an ideal microporous material for mass and heat transfer [21,22]. Despite such attractive properties, well-ordered IOs with varying pore diameters have yet to be examined for their pool boiling heat transfer physics and performance.

In this study, we investigate the boiling curves and heat transfer coefficient *h* of highly-ordered copper IOs through pool

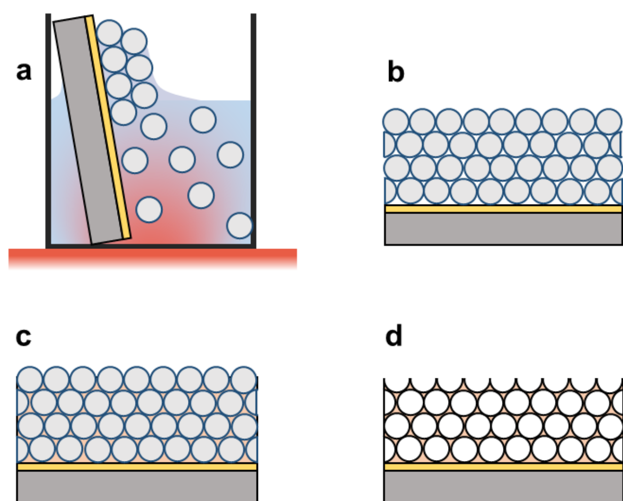

Figure 1. Illustration of copper inverse opals (IOs) fabrication. a) Vertically submerging a functionalized gold substrate in a colloidal suspension allows polystyrene spheres to self-assemble at the evaporating meniscus front. The base heating prevents sphere sedimentation. b) The resulting crystalline opal film anneals in an oven to increase the sphere-to-sphere contact areas. c) Copper electrodeposits into the cavities between the spheres. d) Dissolving the templated spheres with a chemical etchant reveals an IO with highly-ordered and interconnected pores.

boiling conditions. To further understand the effects of pore dimensions on boiling characteristics, we vary the pore diameters of IOs between 0.6 to 1.0 µm by tuning the sacrificial sphere template. We then compare the boiling performance to that of 5.0 µm pore diameter copper IOs presented by Lee *et al.* [22]. A goniometer measures the surface wettability of the copper IO. Scanning electron microscopy (SEM) confirms the crystallinity, porosity, and structural thickness of the IOs while a high-speed camera captures bubble nucleation and departure dynamics at varying heat fluxes.

MATERIAL AND METHODS

Preparation of Copper Inverse Opals. We prepare copper IOs by using sacrificial self-assembled template and electrodeposition to build the inverted metal framework. The process starts with patterning a gold working area (5 x 7 mm^2) with an adhesive layer of titanium on silicon substrate using electron beam evaporation. The working area is functionalized to be hydrophilic by immersing in an aqueous solution of 1 mM sodium 3-mercapto-1-propanesulfonate (Sigma-Aldrich) for a minimum of 24 hr followed by rinsing the substrate with deionized (DI) water and blow-drying with a stream of compressed air. The substrate vertically sits in a 15 mm diameter and 20 mm deep cylindrical well, containing 1.5 mL of aqueous colloidal suspension, which consists of monodispersed polystyrene spheres (Thermo Fisher) where the sphere diameter dictates the pore diameter after the template removal. The colloidal concentration remains at 0.6 %w/v. A hot plate underneath the well promotes uniform gentle

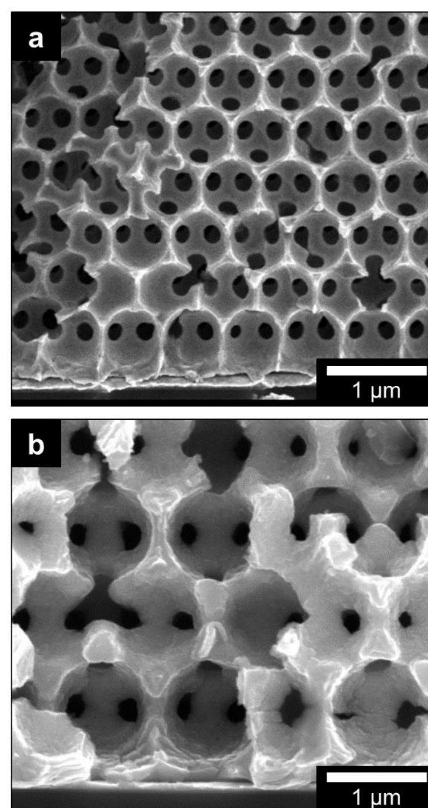

Figure 2. Scanning electron microscope (SEM) images of well-ordered copper IOs. Cross-sectional view of a) 0.6 and b) 1.0 µm pore diameter copper IOs. The IOs are characterized by uniform pore diameters with periodic interconnected windows, denoted as the via.

convective mixing to prevent sphere sedimentation at 55 ± 1°C, as measured with a thermocouple. As the solvent evaporates, the capillary force at the surface meniscus pulls the colloidal particles toward the substrate to self-assemble into hexagonal close-packing arrangement. The resulting colloidal crystal sinters in a radiant oven (Lab-Line) for 5 hr at 98 ± 0.5°C to improve opal structure stability by increasing the sphere-to-sphere contact areas. Afterward, copper electrodeposits into the cavities between the self-assembled spheres and onto bare gold surfaces, using galvanostatic mode (SP-300, Bio-Logic) at a constant current density of 0.53 mA/cm^2 vs. Ag/AgCl reference in a three-electrode chemical cell. A bulk copper electrode and the self-assembled opal structure serve as the counter and working electrode, respectively. The copper electrodeposition process is conducted in an aqueous solution of 0.5 M $CuSO_4$ + 0.1 M H_2SO_4 electrolyte. The thickness of the inverted opal structure can be controlled by the electrodeposition time, which can be confirmed with SEM imaging (FEI Quanta). The polystyrene spheres encased by the copper scaffold are dissolved by immersing in tetrahydrofuran (Sigma Aldrich) for a minimum of one hour. After the sample is thoroughly rinsed with acetone, isopropanol alcohol, and DI water in series, the crystalline morphology is confirmed with SEM imaging.

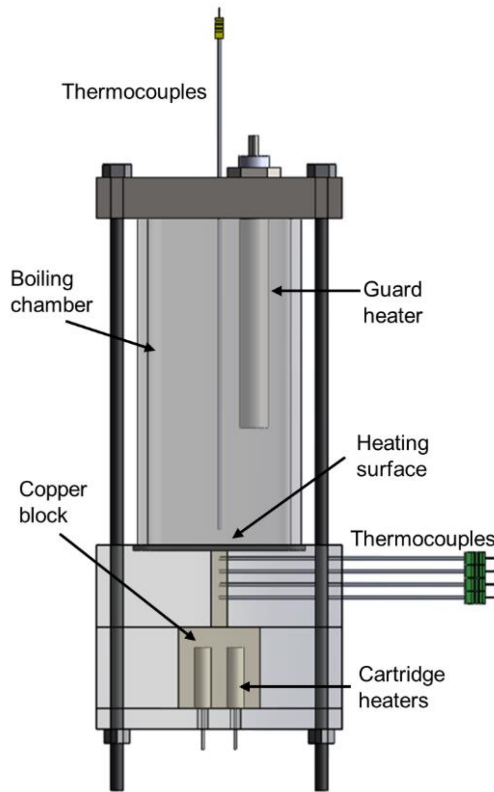

Figure 2. Schematic of pool boiling set-up. The applied power to the cartridge heaters provides heating of the sample. A reservoir of DI water is used as the working fluid in the boiling chamber. Thermocouples monitor the changes in temperature. The transparent boiling

Pool Boiling Measurements. A schematic of the pool boiling set-up is shown in Figure 3. A clear boiling chamber provides direct observation of boiling mechanics while a guard heater ensures that the temperature remains saturated. We use DI water as the working fluid, which is degassed through continuous boiling for ~30 min before using it in the experiment. Cartridge heaters at the base generate heat to the copper block with connected thermocouples monitoring the temperatures through a linked data acquisition system (LabJack). A high-speed camera (Mini FastCam) captures the bubble dynamics at 2,000 fps. The sample is attached to the heating surface by using a thin layer of silver paste. A thin resin of polydimethylsiloxane (PDMS) covers the edges around the substrate to minimize parasitic heat losses. The heat flux of the copper block can be modulated by controlling the applied electric power toward the cartridge heaters. The surface temperature of the heated copper IOs can be estimated using thermal resistance model, assuming uniform one dimensional conduction from the copper block to the surface of copper IOs with a polytetrafluoroethylene (PTFE) base insulating our heaters (Figure 4). In our temperature calculations, q'' is the heat flux, W/m^2; T_1-T_4 are temperature of thermocouple 1-4, °C; T_{Cu} is the temperature of top surface of copper block, °C; t_{1-4} is the distance between T1 and T4, 24.3 mm; t_{sp-1} is the distance between bottom surface of solder paste and T_1, 7.1 mm; T_{Si} is temperature of top surface of silicon wafer; t_{Si} is the

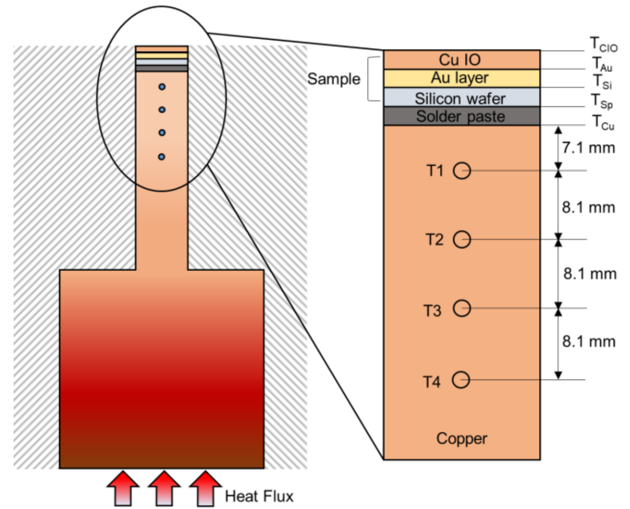

Figure 4. Schematic cross-section of copper block heater. The cartridge heaters provide a heat flux from the copper block base, and the drops in temperatures are measured with thermocouples at discretized locations. A polymer base (gray stripe patterns) surrounding the copper block provides thermal insulation to facilitate one-dimensional conduction heat transfer toward the device surface.

thickness of silicon wafer, 0.5 mm; k_{Si} is the thermal conductivity of silicon, 130 W/mK; t_{Au} is the thickness of gold film, 80 nm; k_{Au} is the thermal conductivity of gold, 314 W/mK; R_{TIM} is the resistance of the thermal interface material (TIM). At each applied heat flux, temperatures are recorded during steady state to produce boiling curves correlating heat flux and wall superheat by using Fourier's Law. The data acquisition system has an uncertainty within ± 0.5 °C.

RESULTS AND DISCUSSIONS

The boiling curves of well-ordered monoporous copper IOs with varying pore diameters between 0.6 and 5.0 µm are plotted

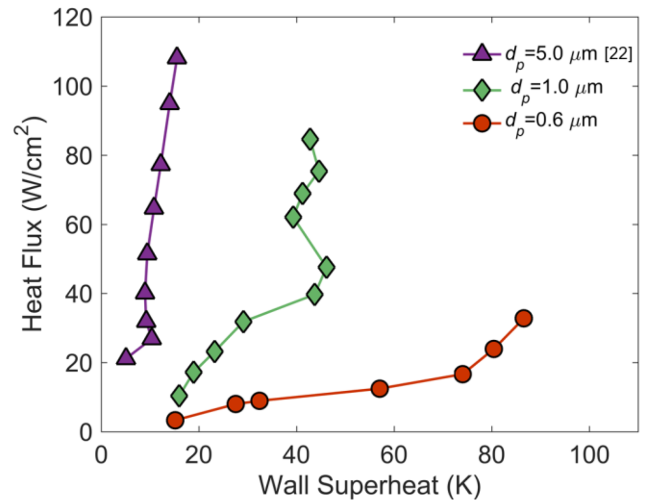

Figure 5. The boiling curves of well-ordered copper IOs with varying pore diameters.

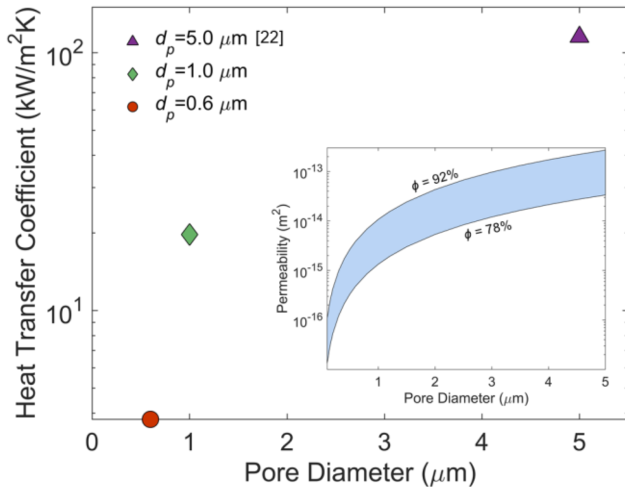

Figure 6. The maximum heat transfer coefficients for 0.6, 1.0, and 5.0 μm pore diameter copper IOs. The inset displays the changes in permeability with pore diameters and porosity as computed through computational fluid dynamics (CFD) simulations. The upper and lower limit of the band is defined by IO porosity of 92% and 78%, respectively.

in Figure 5. The boiling results of 5.0 μm pore diameter copper IO are referenced from Lee *et al*. [22]. In the current work, the CHF has not been reached during pool boiling experiments. Instead, the heat transfer coefficients of IO samples h, defined as the heat flux q'' divided by the wall superheat temperature ΔT_{SH}, are compared for varying pore sizes in Figure 6. This plot shows the maximum heat transfer coefficient h increases with pore diameters. In this study, we expect three major factors contributes to the poor heat transfer performance with excessive superheat temperatures, including 1) the intrinsic nonwetting surfaces of copper IOs, 2) the low permeability in IOs with smaller pores, and 3) thickness of IO samples.

We observe the formation of a thin vapor film that covers the 0.6 and 1.0 μm pore diameter copper IO surface even at low heat fluxes. Over a duration of time, the vapor film evolves to coalesce into one major bubble before departing. Such early advancement to transition and film boiling may be attributed to the low surface wettability of the copper IOs. Sessile droplets of DI water in volume of ~10 nL are pneumatically dispensed (Kyowa) on the copper IO surfaces, revealing intrinsic surface hydrophobicity of approximately 140° in contact angle independent of pore diameters [20]. The surface hydrophobicity favors the formation and departure of vapor while inhibits the returning of cooler liquid to the porous surfaces and consequently further increases the wall superheat temperature ΔT_{SH} [4,23,24], defined as the temperature difference between the top surface of the silicon substrate T_{Si} and saturation temperature of the working fluid T_{sat}. This indicates that a complete dryout occurs within the thickness of the microporous media [5] even at low heat fluxes, as corroborated with the departure of large vapor slugs with diameters of ~6 mm for 0.6 μm pore diameter sample in Figure 7a.

In the case of 1.0 μm pore diameter IO, the improvement in boiling performance may be a result of the larger permeable

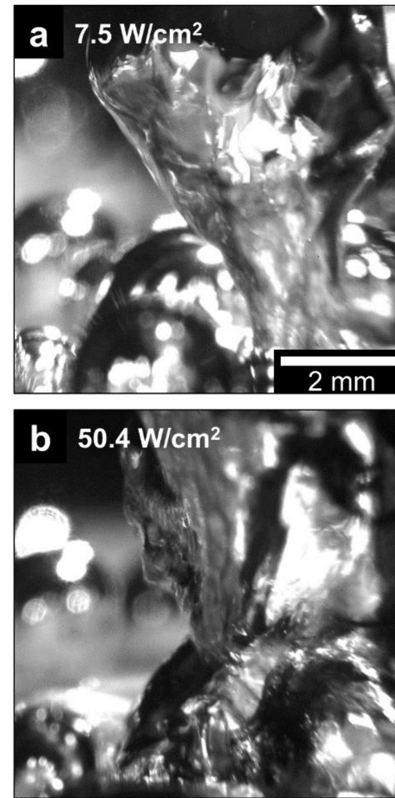

Figure 7. Representative high-speed camera captures of bubble nucleation characteristics for 0.6 μm pore diameter copper IOs at varying heat fluxes. a) At a low heat flux, departing bubbles are ~6 mm in diameter. b) At a high heat flux, vigorous film boiling occurs.

pathway for vapor to escape. The fluid permeability of a porous medium is dependent upon the structural porosity [13], which can be calculated through the quantification of the normalized via diameter d_v/d_p through post-image processing. The value of d_v/d_p can be related to porosity ϕ through a derived analytical expression $\phi=0.58d_v/d_p+0.66$ [20]. The calculated porosity ϕ of IO structure can then be correlated to the its permeability $K=d_p^2(0.07\phi^2-0.0539\phi)$, as determined using computational fluid dynamics (CFD) simulation models. The correlation is valid for $78\% < \phi < 92\%$, and calculation details can be found elsewhere [20]. The IO structure of both 0.6 and 1.0 μm pore diameter possess porosity of ~81%, which results in an estimated permeability K of 9.5 x 10^{-16} and 2.5 x 10^{-15} m^2, respectively. Despite possessing similar porosity and surface wettability, the higher permeability in larger pore diameter IO (i.e., 1.0 μm) allows the bubbles to nucleate and depart at a much faster rate. The effects of higher bubble nucleation and departure rate on boiling heat transfer can be observed by the boiling heat transfer coefficient h in Figure 6. The inset displays the theoretical permeability of IO structure as a function of pore diameters between 0.1 to 5.0 μm over the ranges of porosity. Fluid wicking in porous media is typically governed by the capillary force and viscous resistance [25]. However, due to the impedance of liquid transport through the IOs, the imbalance in mass transport becomes solely dominated by permeability in which vapor can escape. This suggests a correlation between

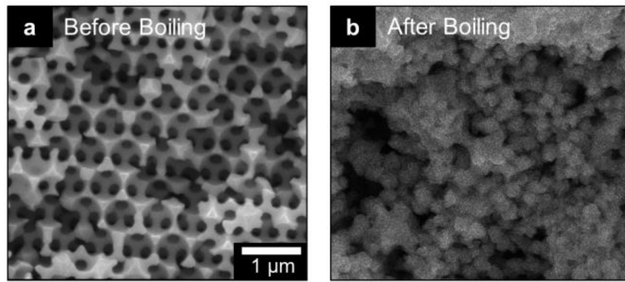

Figure 8. Structural degradation of copper IOs after multiple pool boiling measurements. Top view SEM imaging of 0.6 μm pore diameter IO is shown a) before and b) after 3 trials of testing. Extensive heating and oxidation cause the spherical pore structure to collapse into amorphous features, decreasing the effective porosity.

the permeability of a porous media and its boiling performance exists in the absence of surface rewetting due to the hydrophobicity of the surface, which should be investigated in the future study.

The thicknesses of the copper IO structures are measured to be approximately 21, 17, and 10 μm for 0.6, 1.0, and 5.0 μm pore diameter samples, respectively, as examined through cross-sectional SEM imaging. According to the viscous-capillary model [26], microporous media thickness is a critical parameter in pool boiling heat transfer. The increase in a media thickness decreases the vapor-layer heat flux while increases the CHF but at the expense of excessive wall superheat due to dryout [5]. The large superheat observed for 0.6 μm pore diameter sample can be explained by simple thermal resistance model. Assuming the thermal conductivity of vapor is much smaller than that of the porous copper, the conduction resistance can be expressed as $t_{dry}/(k_{eff}A_{heat})$, where t_{dry} is the vapor layer thickness above the heated surface area, k_{eff} is the effective thermal conductivity of the porous structure, and A_{heat} is the heating area. Due to wicking impedance caused by the hydrophobic IO surfaces, we assume that no evaporation at the liquid-vapor interface occurs within the IO matrix and therefore the convection resistance in the model can be neglected and $t_{dry} \geq t_{IO}$. This simple resistance model shows that thicker IO structures (i.e., in this case, 0.6 μm pore diameter sample) exhibit larger thermal resistance contributed by the vapor film that encompasses the entirety of the IO layer. Decreasing t_{IO} may be a factor that supports the pool boiling enhancement observed in Figure 5 and 6. Previous investigations [27,28] have demonstrated the optimal microporous media thickness for boiling heat transfer is 2-4 times the pore size, which corresponds to t_{IO} of approximately 1-2, 2-4, and 10-20 μm for the 0.6, 1.0, and 5.0 μm pore diameter samples in the study, respectively. Remaining within the prescribed optimal thickness for 5.0 μm pore diameter copper IO may have contributed to its superior two-phase heat transfer performance.

In addition to the heat transfer calculations, we notice the copper IOs experience structural degradation with extensive trials under pool boiling conditions. The surface color of the copper IO optically changes from reddish-brown to dark brown and finally to gray and black with increasing trial number. SEM imaging reveals that the pore structures collapse such that the original well-defined interconnected spherical pore features become amorphous unidentifiable structures (see Figure 8). Additional oxidation layers also decrease the effective pore diameter d_p resulting in the decrease in its permeability. Further thin film analysis using X-ray Photoelectron Spectroscopy (XPS) and Energy Dispersive X-ray (EDX) will identify the changes in surface chemical compositions and explain the thermal stability and reactivity of microporous copper in oxidation-prone environment. The structural durability of metallic microporous media against corrosion needs to be evaluated before they can be used in liquid-vapor phase change thermal management applications.

Further work in varying IO thickness and pore diameter will also establish fundamental thermofluidic properties for crystalline porous media. Improvements in our pool boiling set-up will also enable the investigation of CHF in pool boiling heat transfer.

CONCLUSION

This work demonstrates the saturated pool boiling performance of three-dimensionally ordered copper IOs for varying pore diameters. The increase in IO pore diameters used in this study shows better boiling characteristics, which can be attributed to the combination of hydrophobic surfaces, larger permeable pathways for vapor to escape, and optimization of sample thicknesses. The hydrophobicity of the copper surface prevents liquid from replenishing the IO leading to the prominence of a growing vapor film above the surface. Functionalizing copper at localized areas to be hydrophilic will be necessary to facilitate surface rewetting and minimize the superheat in future work. Another major thermal resistance that contributes to the excessive superheat is the dryout vapor film whose thickness is controlled by the IO thickness, which can be optimized to further enhance the heat transfer rate. The crystallinity of the porous media will provide opportunities for analytical modeling of the fluid flow and heat transfer to explain such phenomenon, enabling the design optimization of metallic IOs for enhanced boiling heat transfer. This work contributes to the development of well-ordered porous media for the next-generation of microfluidic and thermal management devices in two-phase heat transfer.

ACKNOWLEDGMENTS

This work was sponsored by the National Science Foundation (NSF), (CBET-TTP 1643347, Dr. Jose Lage, the Program Director, Thermal Transport Processes). Q.N.P. is grateful for the financial support from the UCI Mechanical and Aerospace Engineering Department Graduate Fellowship. The SEM characterization was performed at the Irvine Materials Research Institute at UCI.

REFERENCES

[1] Palko, J. W., Lee, H., Agonafer, D. D., Zhang, C., Jung, K. W., Moss, J., Wilbur, J. D., Dusseault, T. J., Barako, M., Houshmand, F., Rong, G., Maitra, T., Gorle, C., Won, Y., Asheghi, M., Santiago, J. G. & Goodson, K.

E. High heat flux two-phase cooling of electronics with integrated diamond/porous copper heat sinks and microfluidic coolant supply. *Intersociety Conference on Thermal and Thermomechanical Phenomena in Electronic Systems*. 1511-1517 (2016).

[2] Wei, W., Jian-Hua, D. & Bu-Xuan, W. Boiling heat transfer on surfaces coated by porous wick with vapor channels. *Microscale Thermophysical Engineering*. 5, 277-284 (2001).

[3] Khan, N., Pinjala, D. & Toh, K. C. Pool boiling heat transfer enhancement by surface modification/micro-structures for electronics cooling: a review. *IEEE Electronics Packaging Technology Conference*, Singapore, Singapore, 273-280 (2004).

[4] Ahn, H. S., Lee, C., Kim, H., Jo, H., Kang, S., Kim, J., Shin, J. & Kim M. H. Pool boiling CHF enhancement by micro/nanoscale modification of zircaloy-4 surface. *Nuclear Engineering and Design*. 240, 3350-3360 (2010).

[5] Ha, M. & Graham, S. Pool boiling characteristics and critical heat flux mechanisms of microporous surfaces and enhancement through structural modification. *Appl. Phys. Lett*. 111 (2017).

[6] Rahman, M. M. & McCarthy, M. Boiling Enhancement on Nanostructured Surfaces with Engineered Variations in Wettability and Thermal Conductivity. *Heat Transfer Engineering*. 38, 1285-1295 (2017).

[7] Kosar, A., Kuo, C.-J. and Peles, Y. Boiling heat transfer in rectangular microchannels with reentrant cavities. *Int. J. Heat Mass Transfer*. 48, 4867-4886 (2005).

[8] Zhang, B. J., Kim, K. J. & Yoon, H. Enhanced heat transfer performance of alumina sponge-like nano-porous structures through surface wettability control in nucleate pool boiling. *Int. J. Heat Mass Transfer*. 55, 7487-7498 (2012).

[9] Weibel, J. A., Kousalya, A. S., Fisher, T. S. & Garimella, S. V. Characterization and nanostructured enhancement of boiling incipience in capillary-fed, ultra-thin sintered powder wicks. *InterSociety Conference on Thermal and Thermomechanical Phenomena in Electronic Systems*, San Diego, CA, 2012, pp. 119-129.

[10] Yang, Y., Ji, X., Xu, J. Pool boiling heat transfer on copper foam covers with water as working fluid. *Int. J. Thermal Sciences*. 49, 1227-1237 (2010).

[11] Ranjan, R., Murthy, J. Y. and Garimella, S. V. Bubble dynamics during capillary-fed nucleate boiling in porous media. *InterSociety Conference on Thermal and Thermomechanical Phenomena in Electronic Systems*, San Diego, CA, 2012, pp. 1114-1126.

[12] Satik, C. & Yortsos, Y.C. A pore-network study of bubble growth in porous media driven by heat transfer. *J. Heat Transfer*. 118, 455-462 (1996).

[13] Liter, S. G. and Kaviany, M. Pool-boiling CHF enhancement by modulated porous-layer coating: Theory and experiment. *Int. J. Heat Mass Transfer*. 44, 4287-4311 (2001).

[14] Raimundo, D. S., Hatton, B., Kolle, M. & Aizenberg, J. Self-assembled polystyrene micro-spheres applied for photonic crystals and templates fabrication. *J. Integrated Circuits and System*. 1, 39–43 (2006).

[15] Rengarajan, R., Jiang, P., Larrabee, D., Colvin, V. & Mittleman, D. Colloidal photonic superlattices. *Phys. Rev. B.* 64, 205103–205107 (2001).

[16] Kim, O. et al. Ordered macroporous platinum electrode and enhanced mass transfer in fuel cells using inverse opal structure. *Nature Commun.* 4 (2013).

[17] Kim, D. Y. et al. An electrochemically grown three-dimensional porous Si@Ni inverse opal structure for high-performance Li ion battery annodes. *J. Mater Chem A.* 2, 6396–6401 (2014).

[18] Zhang, C. et al. Characterization of the capillary performance of copper inverse opals. *IEEE Intersociety Conference on Thermal and Thermomechanical Phenomena in Electronic Systems*, Las Vegas, Nevada, USA, 1035–1039 (2016).

[19] Ngo, I. & Chan, B. Permeability of microporous wicks with geometric inverse to sintered particles. *Int. J. Heat Mass Transfer*. 98, 298–302 (2016).

[20] Pham, Q. N., Barako, M. T., Tice, J. & Won, Y. Microscale liquid transport in polycrystalline inverse opals across grain boundaries. *Sci. Rep.* 7 (2017).

[21] Barako, M. T. et al. Quasi-ballistic electronic thermal conduction in metal inverse opals. *Nano Lett.* 16, 2754-2761 (2016).

[22] Lee, H., Maitra, T., Palko, J., Zhang, C., Barako, M., Won, Y., Asheghi, M. & Goodson, K. E. Copper inverse opal surfaces for enhanced boiling heat transfer. *International Technical Conference and Exhibition on Packaging and Integration of Electronic and Photonic Microsystems*. (2017).

[23] Feng, B., Weaver, K. & Peterson, G. P. Enhancement of Critical Heat Flux in Pool Boiling Using Atomic Layer Deposition on Alumina. *Appl. Phys. Lett.* 200, 53120-53123 (2012).

[24] O'Hanley, H., Coyle, C., Buongiorno, J., McKrell, T., Hu, L.-W., Rubner, M. & Cohen, R. Separate Effects of Surface Rougness, Wettability, and Porosity on the Boiling Critical Heat Flux. *Appl. Phys. Lett.* 103, 24102-24106 (2013).

[25] Palko, J. W., Zhang, C., Wilbur, J. D., Dusseault, T. J., Asheghi, M., Goodson, K. E. & Santiago, J. G. Approaching the limits of Two-phase Boiling Heat Transfer: High Heat Flux and Low Superheat. *Appl. Phys. Lett.* 107, 253903-253907 (2015).

[26] Udell, K. S. Heat Transfer in Porous Media Considering Phase Change and Capillarity: The Heat Pipe Effect. *Int. J. Heat Mass Transfer.* 28, 485-495 (1985).

[27] Sarangi, S., Weibel, J. A. & Garimella, S. V. Effect of Particle Size on Surface-Coating Enhancement of Pool Boiling Heat Transfer. *Int. J. Heat Mass Transfer.* 81, 103-113 (2015).

[28] Webb, R. L. Nucleate Boiling on Porous Coated Surfaces. *Heat Transfer Eng.* 4, 71-82 (1983).